Integrated approach to the coronal heating problem

Y. Taroyan

SP^{2}RC, Department of Applied Mathematics, University of Sheffield, Sheffield S3 7RH, UK
email: `y.taroyan@sheffield.ac.uk`

Abstract. Solving the coronal heating problem involves dealing with a number of theoretical and observational steps. These include designing instruments, deriving required observables from observations, developing theories and finding the unique footprints of theoretical models. Each of these steps poses its unique challenges to theoreticians and observers. It is important to treat the heating problem in an integrated manner, whereby each component of the problem is treated in its relationship to the other parts rather than in isolation. The paper presents a brief review of recent developments in the field with an emphasis on forward modeling and inversion which play a central role in solving the heating problem by providing the necessary interaction between theories and observations.

Keywords. Sun: corona, MHD, waves, line: profiles

1. Introduction

The problem of coronal heating has been challenging solar physicists for the past sixty years. Numerous theories have been proposed but none has yet been confirmed. Some of the theories rely on sophisticated models, others merely represent concepts or ideas. The task facing a modern-day physicist is to establish which of these theories (if any) represents the actual heating mechanism or perhaps their combination. For recent reviews see, e.g., Erdélyi (2004), Aschwanden (2005), Klimchuk (2006), Erdélyi & Ballai (2007). Therefore, it is becoming increasingly important to study the signatures and footprints of various heating models or to go even further and make direct comparisons with currently available observational results. Such a forward modeling approach is based on advanced numerical modeling. It narrows down the search for the actual heating mechanism by validating or refuting theoretical models depending on whether or not it is possible to reproduce observations from these models.

Determining the actual physical behavior of the coronal plasma from observables is important for understanding the heating mechanism. The observables are obtained using imagers (Yohkoh/SXT, SoHO/EIT, TRACE, Hinode/SOT/XRT/EIS, STEREO) and spectrometers (SoHO/CDS/SUMER, Hinode/EIS and others). Currently available instruments have limited spatial, temporal and spectral resolution in spite of the advanced technologies used when constructing them. However, inverting the observables is not just an instrumental problem. It is a major theoretical challenge. Helioseismic inversion has been extremely successful in uncovering the physics of the solar interior. It is based on the study of acoustic waves which propagate through the interior. The situation is different in the corona where strong damping, nonlinearity, localization of the structures and other important factors make the problem of inversion much more complicated.

Forward modeling and inversion represent two important and complementary aspects of the heating problem. These two approaches provide an integrated and most efficient currently available way of tackling the heating problem. The present paper briefly

reviews studies which are mainly based on the observational constraints provided by the new generation satellites. The first part deals with the footprints and observational signatures of various heating mechanisms, whereas the second part focuses on the problem of inversion and plasma diagnostics using MHD waves.

2. Observational constraints on theoretical models

Observations since Skylab have shown that the heating of the corona is associated with the magnetic activity of the Sun. Instruments on board SoHO, TRACE, Hinode, etc., show the presence of loop-like magnetic structures. These instruments have different spatial resolution and temperature coverage, so the loops are bound to look different. Active regions account for 82 % of the total coronal heating energy. Therefore, loop modeling is important for understanding the heating mechanism.

In the past few years observations have provided new constraints on theoretical models. A large majority of coronal loops observed by TRACE and EIT (T∼1 MK) were found to be overdense to what would be expected for static equilibrium. The discrepancy was reduced but not eliminated if the heating was assumed to be concentrated near the loop footpoints (Aschwanden et al. 1999, 2001, Winebarger et al. 2003). In contrast, hot (T>2 MK) loops observed by Yohkoh were found to be underdense compared to static equilibrium.

Parker (1988) suggested that the corona is heated by many small and localized bursts of energy. These small scale events are called nanoflares. The nanoflare theory predicts that the loops consist of many thin strands which are beyond the spatial resolution of current space borne or ground based instruments. These strands are wound and wrapped around each other due to the continuous shuffling of their photospheric footpoints. This leads to magnetic reconnection between neighboring strands. According to Parker (1988) the energy released by each event is about 10^{24} erg, hence the term nanoflare (i.e., the average energy of a single event is around 10^{-9} times smaller compared to the energy released during a typical flare). Observations of solar flares indicate a power law for their energy distribution with a slope of about -1.6. However, Hudson (1991) pointed out that for the corona to be heated by nanoflares, the slope would need to be more negative than -2, i.e., the nanoflares must satisfy a different distribution function and, therefore, they may be generated by a different physical mechanism. Transient brightenings detected in short loops were statistically studied by Aschwanden & Parnell (2002). The observations were carried out using TRACE for EUV wavelengths and Yohkoh/SXT for soft X-rays. The statistical distribution of the nanoflare/microflare energies was expressed by a power law with an index of around -1.6 or -1.7. Meanwhile Benz & Krucker (2002) found a power index of less than -2. There have been several other studies, however, no definitive conclusion has been reached at this time (Berghmans 2002).

Analysis of spectral line profiles show that optically thin transition region lines display a net red-shift (see, e.g., Chae et al. 1998; Teriaca et al. 1999a; Peter & Judge 1999; Doyle et al. 2002). These red-shifts are often accompanied by blue-shifts at higher temperature lines. The red-shifts have been observed in coronal holes, quiet sun regions, and active regions. This observational fact has long been recognized as an important clue to the heating process in the solar atmosphere, prompting several authors to build physical models of a remarkably wide variety to try to account for this phenomenon (see, e.g., Mariska 1987; Spadaro et al. 1990; Hansteen 1993; Sarro et al. 1999; Terriaca et al. 1999b). In addition, Doyle et al. (2002) studied the temporal variability in the Doppler shift of transition region lines. High cadence datasets in C III, O VI and Ne VIII were analyzed in an effort to establish the extent of the Doppler shift variability in different

regions of the quiet Sun. Within each of these regions short time-scale variability for the Doppler shift was established. In some cases the line shift could change by 15 km s^{-1} in less than a minute.

The observational constraints on theoretical models are expected to improve with the launch of Hinode, STEREO, SDO and other forthcoming satellites like Solar Orbiter in the pipeline. This will in turn promote forward modeling of possible heating scenarios.

3. Footprints and observational signatures of various heating mechanisms

The great majority of heating theories assume the presence of both small and large scales. Examples of small scales include resonant layers (Ionson 1978; Poedts et al. 1990; Erdélyi & Goossens 1995) and current sheets (van Ballegooijen 1986). The large scales are represented by, e.g., coronal loops. This coexistence poses a severe challenge for multidimensional numerical modeling since an enormous range of scales must be covered. One possible way of dealing with the problem could be the inclusion of a nonuniform grid whereby points are mainly concentrated around small scales. However, many small scale structures get scattered throughout the computational domain as the simulation evolves or could be moved around by flows generated in the system (Ofman & Davila 1996; Erdélyi & Goossens 1996). Another possibility is the use of an adaptive mesh, whereby points are dynamically added or removed. In this case, one has to overcome the problem of the accuracy of the solution at the boundaries between sub-domains with different mesh-size. Currently, many theories rely on one-dimensional modeling to study the plasma response to variations in coronal heating. Simulations of this type, often referred to as loop models, assume that the magnetic field is rigid and plays only a passive role by channeling the plasma and thermal energy along the field lines. One-dimensional models offer the advantage of highly accurate description of the plasma motion along the field lines. All the important effects are incorporated into the energy equation. The disadvantage is the fact that the heating function cannot be determined self-consistently and must be specified in an artificial way (Klimchuk 2006).

One-dimensional models are often used to study the signatures and observational footprints of the nanoflares. Patsourakos & Klimchuk (2005) argued that the diagnostics with current instruments such as TRACE and SXT only weakly depend on the spatial distribution of the heating. TRACE is insensitive to the initial hot temperatures. SXT is sensitive to these temperatures, but the densities and emission measures are small until chromospheric evaporation has had time to fill the loop. The emission is therefore mainly detected during the cooling phase of the strands, long after the nanoflare has occurred. Thermal conduction and mass flows are very efficient at redistributing the energies along the strand so the initial differences are rapidly smoothed out. These arguments were supported by the results of one-dimensional modeling.

Similar conclusions were reached by Cargill & Klimchuk (2004) who found that the initial stages of cooling are dominated by thermal conduction and the later stages are dominated by radiative cooling. The loops were found to be underdense at hot SXT temperatures and overdense at cool TRACE temperatures, in agreement with the observations. They also found a broad emission measure distribution with temperatures from 10^5 to 10^7 K.

TRACE observations show uniform emission of material cooling into the passbands. If the nanoflare model is correct, the new XRT instrument on board the Hinode satellite should register more structured emission along the loop and possibly detect both heating and cooling due to its broad temperature coverage.
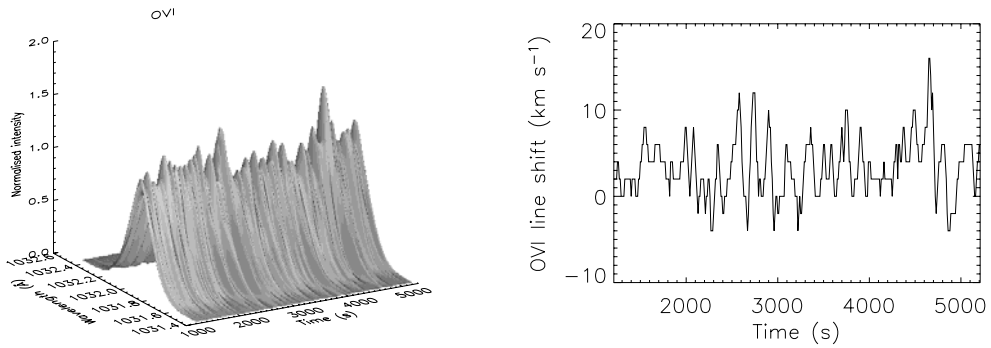
Figure 1. Evolution of the O VI line profile (left) and the corresponding Doppler shift (right) in response to an impulsive heating. The net red shift is about 4.2 km s^{-1} (*from Taroyan et al. 2006.*)

Various aspects of loop heating by random impulses have been studied by Cargill (1994), Walsh et al. (1997), Mendoza-Briceño et al. (2002, 2003, 2005). Taroyan et al. (2006) investigated the evolution of an impulsively heated loop and the spectroscopic consequences of such heating. The nature of these energy depositions is unspecified. They could be signatures of nonlinear wave conversion or reconnection. These energy depositions are represented in the form of episodic heating events randomly deposited along the loop at random times. The effects of gravitational stratification, optically thin radiative losses and thermal conduction are all taken into account. The loop is initially kept at a constant chromospheric temperature of 20 000 K. The initial stage of the loop evolution is completed about 20 min after the start of the nanoflare heating. During this stage the temperature suffers a gradual increase along the loop and the loop is subsequently maintained at coronal temperatures. A narrow and continuously moving transition region is formed. The displacements could be as large as 1 Mm. The accuracy of the solution in the transition region is provided by the adaptive mesh. The results are converted into observable quantities by synthesizing the emission line profiles for C IV, O VI, Ne VIII and Mg X. Figure 1 displays the variation of the O VI line profile and the corresponding Doppler shift. The selected resonant lines have peak formation temperatures covering the upper transition region and lower corona. The study reveals that the impulsive nanoflare heating could account for the observed dynamic behavior of the lines. The model also reproduces the average red-shifts seen in the transition region.

Moriyasu et al. (2004) (see also Kudoh, this volume) studied the propagation of Alfvén waves generated in the photosphere by random motions. The model included the effects of thermal conduction and radiation. A similar type of model was introduced by Hollweg (1982a), (1982b) and applied to the study of spicule formation and heating (see also James & Erdélyi 2002). Moriyasu et al. (2004) found that as the waves propagate upwards they become nonlinear in the chromosphere transition region because of the sharp density decrease and generate slow and fast mode MHD waves and shocks. The plasma is heated at chromospheric heights and the temperature is distributed uniformly along the loop by thermal conduction. The shocks occur one after another leading to episodic heating. Perhaps the most important result of this study is that the distribution of the heating events closely matches the power law distribution of the observed transient brightenings (nanoflares) with an index of around -1.8. For a brief summary of power law indices obtained from observations see Aschwanden (2005) or Erdélyi & Ballai (2007). The model therefore suggests the possibility that the observed nanoflares are not reconnection events

but are actually MHD shock events generated by Alfvén waves. Antolin et al. (this volume) have attempted to find differences in the power law distribution when the loops are heated by Alfvén wave generated MHD shocks and other mechanisms.

Van Doorsselaere et al. (2007) showed that any heating mechanism due to the damping of line-tied oscillations should be dominated by a resistive phenomenon in order to accommodate the constraint of footpoint heating. In contrast to this, mechanisms associated with viscous damping lead to apex heating. They found that the analytical and numerical estimates of the heating scale height for the resonant absorption damping mechanism reproduces the observed scale-height.

Profiles of heating by MHD turbulence were studied by Buchlin et al. (2007). Alfvén waves are excited by granular motions in the photosphere and propagate upwards into the corona where MHD turbulence sets in and the energy cascades from large scales into small scales. They found uniform heating for loops with constant cross-section and footpoint heating in the case of expanding loops. The most important result of their study is the established strong dependence of the average heating profile on the kinetic and magnetic diffusion coefficients. Different profiles of kinematic viscosity and magnetic diffusivity lead to different heating profiles. The heating is enhanced in places where the dominant transport coefficient is enhanced. Goméz & Dmitruk (this volume) have demonstrated that the power law distribution could be a consequence of turbulent heating.

Based on the results of Gudiksen & Nordlund (2005a), (2005b) and Peter et al. (2004), Aschwanden et al. (2007) have argued that observations show no evidence of local heating in the corona. Instead one should be speaking about heating in the upper chromosphere or transition region with subsequent chromospheric evaporation. They presented a number of arguments in support of this idea. A loop that is locally heated in the corona will first brighten up and dim in an EUV filter and subsequently in soft X-ray unless the heating is more rapid than the observing cadence. However, there is little evidence for loop heating being observed in EUV. On the other hand, such behavior could be explained if the heating occurs in the chromosphere / transition region with subsequent chromospheric evaporation. Other arguments include upflows of hot material and downflows of cool material, the overdensity of coronal loops, upward propagating slow waves, the complexity of the magnetic field at low altitudes providing favorable environment for small scale reconnection events such as blinkers, explosive events, transient brightenings, etc., the large loop cross-sections and the current dissipation at transition region heights as evidenced by 3D numerical simulations. The only caveats of the scenario are the nondetection of the initial heating events and the lack of observed upflows.

The above listed results show that reconnection is not the only possibility for heat generation at low altitudes. It is also clear that the footprints of various heating mechanisms often overlap. Therefore, future forward modeling studies must attempt to disentangle the signatures and footprints of various heating scenarios. The forward modeling approach will receive further impetus from the observational constraints which will soon be provided by the new missions.

4. The problem of inversion and diagnostics with MHD waves

Forward modeling is used to derive footprints and observables predicted by various theoretical models. The previous section has shown the difficulties and some of the recent developments in the field. The reverse procedure of deriving the actual footprints and physical quantities from the observations is not easy either. Developing reliable inversion methods is not just an observational task. New theoretical ideas can be rather useful in developing novel inversion techniques.

Perhaps the most well known example of the controversy in the field is a single dataset from which three different temperature and heating profiles along a loop were derived by three different authors: uniform (Priest et al. 1998), footpoint (Aschwanden 2001) and apex (Reale 2002) heating. The discrepancy between the results was mainly attributed to the different ways in which the background was subtracted. Other authors have criticized the assumption of isothermal approximation which is implicit in the conventional filter ratio analysis (Landi & Landini 2005; Schmelz & Martens 2006).

As mentioned in the previous section, most studies have shown lack of evidence for loop heating being observed in EUV. Recently Reale & Ciaravella (2006) have applied the well-known TRACE filter ratio analysis to measure temperature evolution along a loop. The analysis was based on the fact that the loop faded out at the end of the image sequence and so the last images were used to derive a background. The filter ratio (temperature) with no background subtraction remained flat along the loop, whereas the background subtracted images showed temperature structuring with both heating and cooling taking place along the loop. If proven to be correct, these results could present the first real evidence for heating being observed in EUV.

The results of spectroscopic measurements are probably as conflicting as those derived from imagers. Ugarte-Urra et al. (2005) measured the electron density along a coronal loop observed by CDS and EIT. Different approaches for background subtraction were applied. The electron density was determined spectroscopically from the intensity ratio of lines of the same ion. A comparison with the results of a 1D hydrodynamic simulation suggests preferentially footpoint heating. However, other possibilities cannot be ruled out due to the large uncertainties resulting from insufficient spatial and spectral resolution of CDS. Flows not seen by CDS could also change the conclusions. These results are in contrast to the results of Schmelz & Martens (2006) who used the same CDS to study a coronal loop on the limb. They found broad DEM distributions for a number of pixels both before and after the background subtraction was applied. They also found temperature variation along the loop from the footpoint to the apex in contrast to the results derived from TRACE and EIT.

New instruments will provide further insight and perhaps reconcile the discrepancies which currently exist. The XRT instrument on board the Hinode satellite gives the opportunity to construct thermal maps using 5 or more filters.

An alternative approach to the inversion problem could be the use of MHD waves. MHD waves are an excellent diagnostic tool and their full potential has yet to be explored. Most of the works in the present volume are dedicated to this problem. MHD waves could be used for a number of purposes: measuring the magnetic field strength, the fine structure, the transport coefficients in the solar atmosphere, understanding the processes responsible for the damping of these waves and so on (see, e.g., De Moortel et al. 2000; Nakariakov & Ofman 2001; Goossens et al. 2002; Ruderman & Roberts 2002; Díaz et al. 2002; Zaqarashvili T. V. 2003; Ruderman & Erdélyi 2004; Andries et al. 2005; Ballai et al. 2005; Dymova & Ruderman 2005; Erdélyi & Carter 2006; Erdélyi & Fedun 2006; Erdélyi & Verth 2007; Verth et al. 2007; Carter & Erdélyi 2007; O'Shea et al. 2007; Jess et al. 2008). For more details on the observed MHD waves, their damping, etc., see Nakariakov & Verwichte (2005), Banerjee et al. (2007).

Quantifying the heating function is important for understanding the nature of the heating mechanism. In this respect, standing acoustic waves detected by Kliem et al. (2002), Wang et al. (2002) in hot active region loops could be quite useful. The damping of these oscillations was studied by Ofman & Wang (2002), Mendoza-Briceño et al. (2005), Selwa et al. (2005), Luna-Cardozo et al. (this volume). Observations show that these waves are usually preceded by footpoint brightenings. Taroyan et al. (2005) have
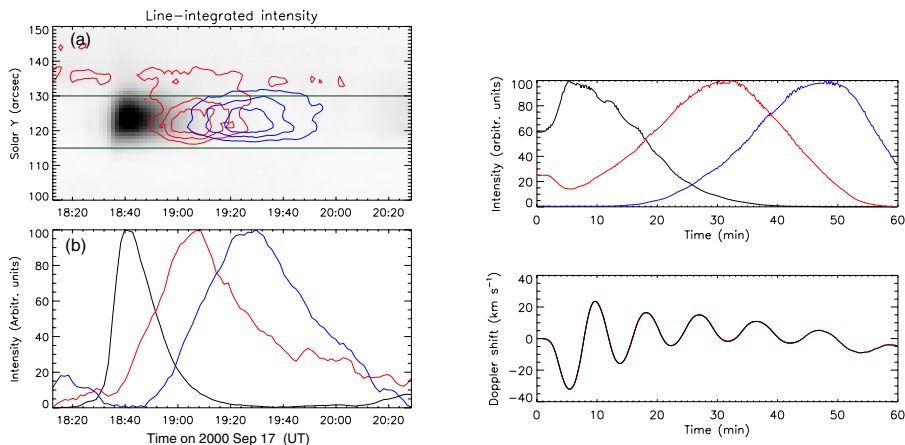
Figure 2. Left - SUMER observations: the top panel represents the time series of the Fe xix (black) line intensity along the slit. The overlaid contours represent the Ca xv ($\lambda\,1098$, red) and Ca xiii (blue) intensity time series. The contour levels are 70, 80, and 90% of the peak intensity; the bottom panel is the average time profile of line-integrated intensity along the cut in the top panel. Right - synthesized observations: the top panel shows the simulated time profiles of the line intensities along the slit cut. The black, red and blue lines correspond to Fe xix , Ca xv ($\lambda\,1098$), and Ca xiii intensities; the bottom panel shows the corresponding Doppler shift (*from Taroyan et al. 2007a.*)
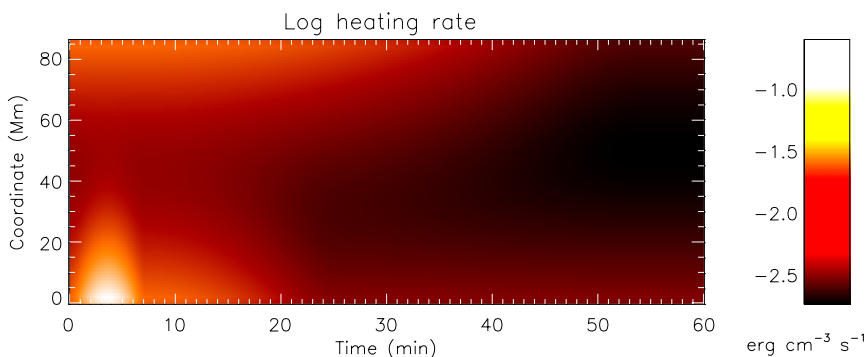

Figure 3. The heating rate (in logarithmic scale) as a function of time and coordinate along the observed loop. The brightening at the lower footpoint corresponds to the microflare which initiates the fundamental mode standing wave. (*from Taroyan et al. 2007a.*)

analytically derived the mathematical form of the heating pulse required to rapidly set up a standing wave. The main requirement is that the duration of the heating pulse approximately matches the period of the oscillations. Taroyan et al. (2007a) applied these results to the study of a real example in an active region. An 86 Mm long loop underwent heating to $T \approx 7$ MK followed by cooling to $T \approx 2$ MK in less than two hours. The heating was followed by a rapidly damped oscillation with a period of about 8 minutes. The maximum initial Doppler shift registered by SUMER was about 30 km s^{-1}. Hydrodynamic simulations were performed using the parameters of the observed loop and including the thermal and radiative losses in the energy equation. The simulation results were converted into observables by applying spectral line synthesis. The comparison between the simulated and observed line profiles was done in three different lines which cover temperatures from 3 to 7 MK.

Figure 2 compares the simulated line profiles with the actual SUMER measurements. In both cases, each line suffers an intensity increase followed by a decrease. The initial increase in the Fe XIX line intensity is a consequence of the footpoint brightening seen by Yohkoh/SXT and the corresponding temperature increase. The subsequent decrease represents the cooling phase. The intensities of the cooler Ca XV and Ca XIII lines consecutively pass through their peaks as the loop cools to lower temperatures. The oscillations only appear in the Doppler shift. The initial negative blue shift of about 32 km s^{-1} is followed by a damped oscillation. A successful comparison between the observed and simulated loop behavior allowed Taroyan et al. (2007a) to

(*a*) establish the nature of the observed oscillations in terms of a fundamental mode standing acoustic wave;

(*b*) confirm that the waves are excited by a microflare occurring at one of the loop footpoints and estimate its energy;

(*c*) determine the evolution of the heating rate along the loop.

Figure 3 displays the inferred time-distance plot for the heating rate (in logarithmic scale). The brightening at the lower footpoint corresponds to the microflare. The heating rate decreases to 20% of its initial value at the bottom (northern) footpoint within about 25 min. It also decreases to 10% of the initial value at the top (southern) footpoint but on a longer time scale so as to gradually change the net red shift into blue shift.

It is not yet clear why these oscillations are only being seen in high temperature lines. Taroyan & Bradshaw (2007) have shown that standing waves can be formed in cooler EUV loops in a similar way when all the important effects such as gravitational and thermal stratification, losses, etc., are taken into account. Hot loops are therefore not unique in this respect and there is nothing to prevent the formation of standing waves in cooler loops. Both standing and propagating waves are a natural response of the loop plasma to impulsive heating. The simulation results are presented in terms of synthetic Hinode/EIS observations to predict the wave footprints in the actual observations. In the case of imaging mode observations with the 40″ slot, the waves are most clearly seen in the EIS Fe XII 195 Å filter when they are just being set up. In contrast to this, the waves clearly appear in all three lines when spectroscopic observations with the 1″ slit are applied. There is a quarter period phase shift between the intensity and the Doppler shift oscillations indicating the presence of a standing wave. The intensity oscillations suffer phase variations when the plasma undergoes heating or cooling.

It must be mentioned that individual standing waves are not very often seen. Another interesting possibility for reliable inversion may come from the analysis of Doppler shift time series. The idea proposed by Taroyan et al. (2007b) is borrowed from helioseismology where the use of such time series has become a routine method for extremely precise diagnostics of the solar interior. The new method does not require the presence of coherent standing waves. The only underlying assumption is that the loops (or strands) are heated randomly both in time and in space (an argument supported by the results presented in the previous section). The analytical study shows that for a linear ideal 1D loop model heated by random pulses there is an infinite number of peaks in the velocity power spectrum corresponding to the frequencies of standing waves. The inclusion of radiative losses, thermal conduction and nonlinearity introduces noise in the power spectrum. The most prominent peak corresponding to the fundamental mode is always present regardless of the random heating function and the heliographic position of the loop. This peak could therefore be used to determine the average temperature of the plasma inside the loop. The peak corresponding to the second harmonic only appears in the case of uniformly random heating. Peaks corresponding to the higher harmonics do not show up due to their small amplitudes, losses and nonlinearity. The results of the wavelet analysis for
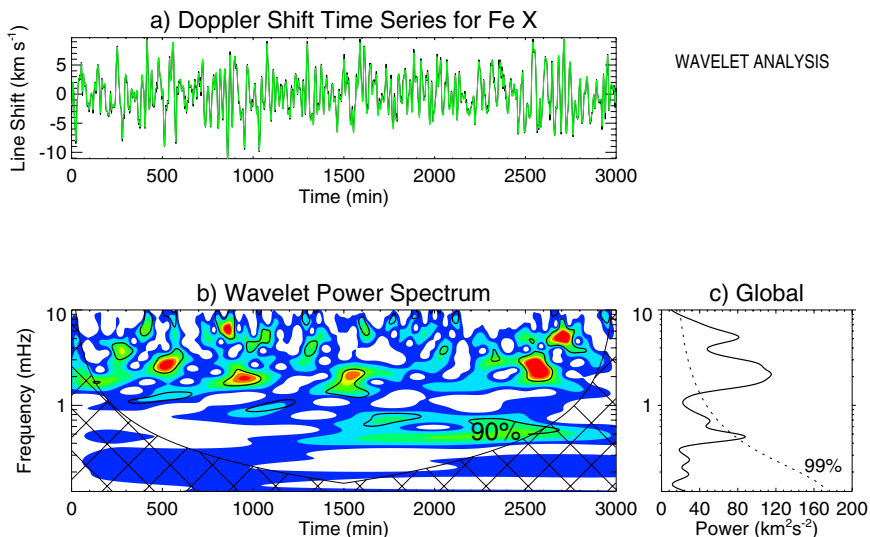
Figure 4. Wavelet analysis results corresponding to uniformly random heating along a 30 Mm long loop. The top panel (a) shows the Doppler shift time series in the Fe x line. The bottom left panel (b) displays the wavelet power spectrum. The red color represents high power and the blue color corresponds to low power. The bottom right panel (c) is the global wavelet spectrum. In the wavelet spectrum diagram (b), regions with 90% significance level are outlined in black. In the global wavelet diagram, the dotted lines indicate 99% significance level.

such a loop are displayed in Figure 4. Loops heated near their footpoints only display the fundamental mode. This is mainly due to the large values of thermal conduction around the maximum of the second harmonic which results in strong damping. The phenomenon is explained in more details by Taroyan et al. (2007b). The power spectrum analysis could therefore be used to establish the spatial distribution of the random heating. The power spectra are also sensitive to the temporal distribution of heating and, as a result, they could be used to estimate the average amount of energy involved in a single heating event. Interestingly, the peaks do not show up when the same analysis is applied to the intensity time series. This effect as well as the previously mentioned phase shifts in the synthesized EIS observations are analytically explained by Taroyan & Bradshaw (2007).

5. Summary

- Forward modeling and inversion are two complementary approaches which allow the heating problem to be tackled in an integrated and comprehensive manner.
- The new generation satellites have provided new constraints on theoretical models and triggered a wealth of studies which focus on the footprints and observable consequences of various theoretical heating scenarios.
- These footprints often overlap with each other. Therefore future research is facing the task of disentangling the footprints in order to distinguish the predictions of various heating mechanisms.
- Recent and future missions (Hinode, STEREO, SDO) are most likely to provide further stringent constraints and trigger a new race in theoretical forward modeling.

• Being equipped with coordinated diagnostic capabilities, these missions are also expected to improve our understanding of the coronal plasma.

• New inversion methods based on MHD waves are being developed. These methods have the potential to compete and serve as alternative to more conventional techniques

• Standing longitudinal (acoustic type) waves in coronal loops are important for quantifying the unknown heating function. The analysis of Doppler shift time series is a new efficient tool for determining the spatial and temporal distribution of the heating function. The method does not require the presence of individual coherent waves.

Acknowledgements

References

Andries J., Arregui I., & Goossens M., ApJ 624, L57 (2005)
Antolin P, Shibata K., Shiota D., & Brooks D., in R. Erdélyi and C.A. Mendoza-Briceño (eds.) *Waves & Oscillations in the Solar Atmosphere: Heating and Magneto-seismology*, IAU Symposium, 247, 281 (2008)
Aschwanden M. J., A&A 560, 1035 (2001)
Aschwanden M. J., Physics of the Solar Corona (New York: Springer) (2005)
Aschwanden M. J., Newmark J. S., Delaboudiniere J.-P. et al., ApJ 515 842 (1999)
Aschwanden, M. J., & Parnell, C. E., ApJ 572, 1048 (2002)
Aschwanden M. J., Schrijver C. J., Alexander D., ApJ 550 1036 (2001)
Aschwanden M. J., Winebarger A., Tsiklauri D., Peter H., ApJ 659, 1673 (2007)
Ballai I., Erdélyi R., Pintér B., ApJ 633, L145 (2005)
Banerjee, D.; Erdélyi, R., Oliver, R., O'Shea, E., Sol. Phys., 246, 3 (2007)
Benz A. O., Krucker S., ApJ 568, 413 (2002)
Berghmans D., ESA-SP 506, 501 (2002)
Buchlin E., Cargill P. J., Bradshaw S. J., Velli M., A&A 469, 347 (2007)
Cargill, P. J., ApJ 422, 381 (1994)
Cargill, P. J. & Klimchuk J. A., ApJ 605, 911 (2004)
Carter B. K., & Erdélyi R., A&A 475, 323 (2007)
Chae J., Yun H. S., & Poland A. I., ApJS 114, 151 (1998)
De Moortel I., Ireland J., & Walsh R.W., A&A 355, L23 (2000)
Díaz A. J., Oliver R., & Ballester J. L., ApJ 580, 550 (2002)
Doyle J. G., Madjarska M. S., Roussev I., Teriaca L., Giannikakis J., A&A, 396, 255 (2002)
Dymova M. V., & Ruderman M. S., Sol. Phys. 229, 79 (2005)
Erdélyi R., A&G 45, 34 (2004)
Erdélyi R., & Ballai, I., Astron. Nacht. 328, 726 (2007)
Erdélyi R., & Carter B. K., A&A 455, 361 (2006)
Erdélyi R., & Fedun V., Sol. Phys. 238, 41 (2006)
Erdélyi R., & Goossens, M., A&A 294, 575 (1995)
Erdélyi R., & Goossens, M., A&A 313, 664 (1996)
Erdélyi R., & Verth G., A&A 462, 743 (2007)
Gómez D., & Dmitruk P., in R. Erdélyi and C.A. Mendoza-Briceño (eds.) *Waves & Oscillations in the Solar Atmosphere: Heating and Magneto-seismology*, IAU Symposium, 247, 271 (2008)
Goossens M., Andries J., & Aschwanden M. J., A&A 394, L39 (2002)
Gudiksen B. V., & Nordlund A., ApJ 618, 1020 (2005a)
Gudiksen B. V., & Nordlund A., ApJ 618, 1031 (2005b),
Hansteen, V. H., ApJ 402, 741 (1993)
Hollweg J. V., ApJ 254, 806 (1982a)

Hollweg J. V., ApJ 257, 345 (1982b)

Hudson H. S., Sol. Phys. 133, 357 (1991)

Ionson J. A., ApJ 226, 650 (1978)

James, S. P. & Erdélyi R., A&A 393, L11 (2002)

Jess, D., Mathioudakis, M., Keenan, F.P., Erdélyi, R., Verth, G. & McAteer, R.T.J. ApJ, in press (2008)

Kliem B., Dammasch I. E., Curdt W., & Wilhelm K., ApJ 568, L61 (2002)

Klimchuk J. A., Sol. Phys. 234, 41 (2006)

Kudoh, T., in R. Erdélyi and C.A. Mendoza-Briceño (eds.) *Waves & Oscillations in the Solar Atmosphere: Heating and Magneto-seismology*, IAU Symposium, 247, 197 (2008)

Landi E., & Landini M., ApJ 618, 1039 (2005)

Luna-Cardozo, M., Erdélyi, R. & Mendoza-Briceño, C.A., in R. Erdélyi and C.A. Mendoza-Briceño (eds.) *Waves & Oscillations in the Solar Atmosphere: Heating and Magneto-seismology*, IAU Symposium, 247, 318 (2008)

Mariska, J. T., ApJ 319, 465 (1987)

Mendoza-Briceño, C. A., Erdélyi, R., Sigalotti, L. Di G., ApJ 579, L49 (2002)

Mendoza-Briceño, Sigalotti, L. Di G., C. A., Erdélyi, R., AdSpR 32, 995 (2003)

Mendoza-Briceño, Sigalotti, L. Di G., C. A., Erdélyi, R., ApJ 624, 1080 (2005)

Moriyasu S., Kudoh T., Yokoyama T., & Shibata K., ApJ, 601, L107 (2004)

Nakariakov V. M., & Ofman L., A&A 372, L53 (2001)

Nakariakov V. M., & Verwichte E., LRSP 2, 3 (2005)

Ofman L., Davila J. M., ApJ 456, L123 (1996)

Ofman, L., & Wang, T. J., ApJ 580, L85 (2002)

O'Shea E., Srivastava A. K., Doyle J. G., Banerjee, D., A&A 473, L13 (2007)

Parker E. N., ApJ 330, 380 (1988)

Patsourakos S., & Klimchuk J. A., ApJ 628, 1023 (2005)

Peter, H., Judge, P. G., ApJ, 522, 1148 (1999)

Peter H., Gudiksen B., & Nordlund A., ApJ 617, L85 (2004)

Poedts S., Goossens M., & Kerner W., ApJ 360, 279 (1990)

Priest E. R., Foley C. R., Heyvaerts J., et al., Nature 393, 545 (1998)

Reale F., ApJ 580, 566 (2002)

Reale F., Ciaravella A., A&A 449, 1177 (2006)

Ruderman M. S., & Erdélyi R., in (sci-eds) R. Erdélyi, J. L. Ballester, B. Fleck, *Waves, Oscillations and Small-Scale Transient Events in the Solar Atmosphere: A Joint View from SOHO and TRACE*, ESA-SP 547, 507 (2004)

Ruderman M. S., & Roberts B., ApJ 577, 475 (2002)

Sarro, L. M., Erdélyi, R., Doyle, J. G., Pérez, M. E., A&A 351, 721 (1999)

Selwa M., Murawski K., Solanki S. K., A&A 436, 701 (2005)

Schmelz J. T., & Martens P. C. H., ApJ 636, L49 (2006)

Spadaro, D., Noci, G., Zappalà, R., & Antiochos, S. K., ApJ, 355, 342 (1990)

Taroyan Y., & Bradshaw, S. J. A&A, in press (2007)

Taroyan, Y., Bradshaw, S. J., & Doyle, J. G., A&A 446, 315 (2006)

Taroyan Y., Erdélyi, R., Doyle, J. G., & Bradshaw, S. J., 2005, A&A, 438, 713

Taroyan Y., Erdélyi R., Doyle J. G., Bradshaw S. J., A&A 462, 331 (2007b)

Taroyan Y., Erdélyi R., Wang T. J., Bradshaw S. J., ApJ 659, L173 (2007a)

Teriaca, L., Banerjee, D., Doyle, J. G., A&A 349, 636 (1999a)

Teriaca, L., Doyle, J. G., Erdélyi, R., & Sarro L. M., A&A 352, L99 (1999b)

Ugarte-Urra I., Doyle J. G., Walsh R. W., Madjarska M. S., A&A 439, 351 (2005)

van Ballegooijen A. A., ApJ 311, 1001 (1986)

van Doorsselaere T., Andries J., Poedts S., A&A 471, 311 (2007)

Verth, G., van Doorsselaere, T., Erdélyi, R., Goossens, M., A&A 475, 341 (2007)

Wang, T. J., Solanki, S. K., Curdt, W., Innes, D. E., & Dammasch, I. E., ApJ 574, L101 (2002)

Walsh, R. W., Bell, G. E., Hood, A. W., Solar Phys. 171, 81 (1997)

Winebarger A. R., Warren H. P., Mariska J. T., ApJ 587 439 (2003)

Zaqarashvili T. V., A&A 399, L15 (2003)